Journal of Biomolecular NMR, 10 (1997) 9–19

J-Bio NMR 444

Assignments, secondary structure and dynamics of the inhibitor-free catalytic fragment of human fibroblast collagenase

Franklin J. Moy[a], Michael R. Pisano[b], Pranab K. Chanda[b], Charlotte Urbano[b], Loran M. Killar[c], Mei-Li Sung[c] and Robert Powers[a,*]

Departments of [a]Structural Biology, [b]Core Biotechnology and [c]Endothelial and Cytokine Biology, Wyeth-Ayerst Research, Pearl River, NY 10965, U.S.A.

Received 28 January 1997
Accepted 4 March 1997

Keywords: Matrix metalloproteinase; Collagenase; Multidimensional NMR; Resonance assignments; Secondary structure; Backbone dynamics

Summary

Fibroblast collagenase (MMP-1), a 169-residue protein with a molecular mass of 18.7 kDa, is a matrix metalloproteinase which has been associated with pathologies such as arthritis and cancer. The assignments of the ^{1}H, ^{15}N, ^{13}CO and ^{13}C resonances, determination of the secondary structure and analysis of ^{15}N relaxation data of the inhibitor-free catalytic fragment of recombinant human fibroblast collagenase (MMP-1) are presented. It is shown that MMP-1 is composed of a β-sheet consisting of five β-strands in a mixed parallel and antiparallel arrangement (residues 13–19, 48–53, 59–65, 82–85 and 94–99) and three α-helices (residues 27–43, 112–124 and 150–160). This is nearly identical to the secondary structure determined from the refined X-ray crystal structures of inhibited MMP-1. The major difference observed between the NMR solution structure of inhibitor-free MMP-1 and the X-ray structures of inhibited MMP-1 is the dynamics of the active site. The 2D ^{15}N-^{1}H HSQC spectra, the lack of information in the ^{15}N-edited NOESY spectra, and the generalized order parameters (S^2) determined from ^{15}N T_1, T_2 and NOE data suggest a slow conformational exchange for residues comprising the active site (helix B, zinc ligated histidines and the nearby loop region) and a high mobility for residues Pro^{138}-Gly^{144} in the vicinity of the active site for inhibitor-free collagenase. In contrast to the X-ray structures, only the slow conformational exchange is lost in the presence of an inhibitor.

Introduction

Fibroblast collagenase (MMP-1) is a member of the matrix metalloproteinase (MMP) family, which includes the collagenases, stromelysins and gelatinases (Woessner, 1991; Morphy et al., 1995; Ries and Petrides, 1995). These enzymes require zinc and calcium for activity (Lowry et al., 1992; Feng et al., 1995; Springman et al., 1995) and are modular with both propeptide and catalytic domains being common to the entire family (Goldberg et al., 1986; Muller et al., 1988). The physiological function of these enzymes is the degradation of the extracellular matrix which is associated with normal tissue remodeling processes such as pregnancy, wound healing and angiogenesis (Woessner, 1991). Because of the degradative nature of these enzymes, the MMPs are highly regulated by either specific inhibitors (tissue inhibitor of metalloendoproteases – TIMP), by cleavage of the inactive proenzyme or by transcription induction or suppression (Ries and Petrides, 1995). A number of biochemical stimuli including cytokines, hormones, oncogene products and tumor promoters affect the synthesis and activation of MMPs. Therefore, the MMPs have been implicated in a variety of diseases caused by uncontrolled matrix degradation, including tumor metastasis, osteoarthritis and rheumatoid arthritis, corneal ulceration and periodontitis (Grymes et al., 1993). As a result, the MMPs are a prime target for structure-based drug design.

There have been a number of X-ray and NMR structures solved for the MMPs' catalytic domain complexed with a variety of inhibitors (Gooley et al., 1993,1994, 1996; Van Doren et al., 1993,1995; Bode et al., 1994;

*To whom correspondence should be addressed.
Supplementary material available from the authors: one table containing the ^{1}H, ^{15}N, ^{13}CO and ^{13}C resonance assignments for collagenase.

Borkakoti et al., 1994; Lovejoy et al., 1994a; Spurlino et al., 1994; Stams et al., 1994; Becker et al., 1995; Feng et al., 1995; Botos et al., 1996; Broutin et al., 1996) and a crystal structure of collagenase complexed to itself (Lovejoy et al., 1994b). However, because of the proteolytic nature of these enzymes and the resulting self-cleavage and degradation, structural information of inhibitor-free MMPs is not readily available. Since valuable structural information can be obtained from understanding any conformational change induced in the enzyme upon inhibitor binding, a structural program to determine the high-resolution NMR solution structure of inhibitor-free collagenase was initiated.

Here, we report the near-complete ^{1}H, ^{15}N, ^{13}CO and ^{13}C assignments of the spectrum of the inhibitor-free catalytic fragment of human fibroblast collagenase (MMP-1) from a series of 3D triple-resonance experiments. These assignments have led to the determination of the solution secondary structure for MMP-1 based on NOE data involving the NH, H^{α} and H^{β} protons as well as $^{3}J_{HN^{\alpha}}$ coupling constants, amide exchange and $^{13}C^{\alpha}$ and $^{13}C^{\beta}$ secondary chemical shifts and the analysis of the dynamics of MMP-1 based on order parameters (S^2) determined from ^{15}N T_1, T_2 and NOE data. Three crystal structures have been reported for MMP-1 bound to inhibitors, where the protein is composed of a five-stranded β-sheet and three α-helices and the inhibitor is bound to the catalytic zinc in the active site. Comparison between the NMR secondary structure and the refined X-ray structures indicates nearly identical secondary structures; however, a region near the active site in the inhibitor-free NMR structure is highly mobile and residues comprising the active site appear to undergo slow conformational exchange which is lost upon binding an inhibitor.

Materials and Methods

Expression of recombinant ^{15}N- and $^{13}C/^{15}N$-labeled MMP-1

A 169-residue C-terminally truncated human fibroblast collagenase (MMP-1) was expressed in *E. coli*. The coding sequence of a C-terminally truncated procollagenase was amplified by PCR from the plasmid, pNOT-3A, that contains the entire coding sequence of MMP-1 (Goldberg et al., 1986). The PCR primers contained the appropriate restriction sites for ease of cloning. The construct codes for a truncated proMMP-1 with an N-terminal methionine added and a C-terminal proline at residue 250 of the native proMMP-1 sequence. The PCR amplified DNA fragment was then cloned into pET-21a(+) vector at the Nde I/Sal I sites, resulting in a recombinant plasmid designated as mCL-t. *E. coli* bacteria, BL21(DE3), containing the plasmid mCL-t, were grown in LB broth supplemented with 100 mg/ml ampicillin. An overnight culture was diluted 1:20 and grown at 37 °C to an A_{600} of 0.6–0.8 with vigorous shaking. Isopropyl β-D-thiogalactoside (IPTG) was added to a final concentration of 1 mM and cultures were shaken for 3 h at 37 °C. The cells were harvested by centrifugation (7000 × g for 20 min) at 4 °C, washed with PBS and frozen at −70 °C.

Uniform ^{15}N- and ^{13}C-labeled mCL-t was obtained by growing BL21(DE3) *E. coli* in defined media containing 2.0 g/l [^{13}C6,98%+]D-glucose and 1.25 g/l [^{15}N,98%+]ammonium chloride as the sole carbon and nitrogen sources, respectively. In addition, the defined media contained M9 salts (Sambrook et al., 1989), trace elements, vitamins and 100 μg/ml ampicillin. Conditions for induction and growth were the same as above.

Purification of recombinant ^{15}N- and $^{13}C/^{15}N$-labeled MMP-1

MMP-1 was purified according to Spurlino et al. (1994) with modifications as follows. Frozen cell pellets were thawed on ice. Cells were resuspended by homogenization in lysis buffer (0.1 M Tricine, pH 8.0, 10 mM EDTA, 2 mM DTT, 0.2 mM PMSF) and lysed by treatment with lysozyme (1 mg/ml final) at room temperature for 30 min. The lysate was incubated at 37 °C for 15 min in the presence of 0.5% Brij-35, 20 mM $MgCl_2$ and 20 μg/ml Dnase I. The lysate was centrifuged at 48 000 × g for 20 min and the above treatment was repeated on the resultant pellets. The final pellet was washed twice with 50 mM Tricine, pH 7.5, 0.2 M NaCl, 10 mM $CaCl_2$, 0.02% NaN_3, 2.0 mM DTT, 0.2 mM PMSF, resuspended in fresh urea buffer (20 mM Tricine, pH 7.5, 6 M urea, 5 mM $CaCl_2$, 0.02% NaN_3) plus 2 mM DTT and incubated at room temperature for 1 h. The urea solubilized protein was centrifuged at 48 000 × g for 45 min and the resultant supernatant was filtered and applied to a Mono-Q anion exchange column equilibrated in urea buffer. The column was washed with urea buffer and eluted with a 0–0.25 M NaCl linear gradient. Fractions containing proMMP-1 were detected by SDS-PAGE, pooled and quickly diluted into 10-fold excess of renaturing buffer (50 mM Tricine, pH 7.5, 0.4 M NaCl, 10 mM $CaCl_2$, 0.1 mM $ZnOAc_2$, 0.02% NaN_3). After 2 days of dialysis against 25 volumes of renaturing buffer (with three changes), refolded proCL-t was concentrated to about 4 mg/ml in a Centriprep 10 concentrator. The sample was aliquotted and stored at −70 °C. ProCL-t was activated to mCL-t (mature CL-t) by an overnight incubation at 37 °C in the presence of 1 mM *p*-aminophenylmercuric acetate (APMA). The activated protein is then applied to a Superdex-75 16/60 gel filtration column equilibrated in 2.5 mM Tris-HCl, pH 7.5, 5 mM $CaCl_2$, 0.4 M NaCl, 0.02% NaN_3 and 0.05 mM $ZnOAc_2$. The protein is eluted and fractions containing mCL-t were identified by SDS-PAGE. Peak fractions were pooled and the protein was concentrated in a Centriprep 3 concentrator to about 7 mg/ml and stored at −70 °C. N-terminal amino acid sequencing was performed to confirm the protein's identity. The uniform ^{15}N and ^{13}C

labeling of mCL-t was confirmed by MALDI-TOF mass spectrometry.

Effects of pH and buffer composition on MMP-1 activity

Studies on the effect of pH on MMP-1 activity were performed using 10 mM Bis-Tris buffer with 5 mM $CaCl_2$, 100 mM NaCl, 0.1 mM $ZnCl_2$ and 2 mM NaN_3, at pH values 7.5, 7.0, 6.5 and 6.0. Activities of the enzyme in either 10 mM Bis-Tris or Tris-base with the additional components listed above were compared at pH values 7.5 and 7.0. In addition, the enzyme activity was monitored in the presence of DTT (0–10 mM) with an enzyme concentration range of 28–81 nM. Enzyme activity was assessed in a kinetic assay using nonlabeled recombinant MMP-1 described above and a peptide substrate (Weingarten and Feder, 1985).

NMR sample preparation

Samples of $^{13}C/^{15}N$- and ^{15}N-labeled collagenase in 90% H_2O/10% D_2O were prepared by concentration and buffer exchange using Millipore Ultrafree-10 centrifugal filters. Protein was exchanged into a buffer containing 10 mM deuterated Tris-base, 100 mM NaCl, 5 mM $CaCl_2$, 0.1 mM $ZnCl_2$, 2 mM NaN_3, 10 mM deuterated DTT, 90% H_2O/10% D_2O and pH 6.5. $^{13}C/^{15}N$-labeled collagenase in 100% D_2O was prepared similarly until the H_2O concentration was about 10 mM. Sample concentrations were 1 mM determined spectrophotometrically using an extinction coefficient of 24 800 M^{-1} cm^{-1} at 280 nm. Sample conditions were identical for the collagenase–inhibitor complex (1:1).

DTT was required for stability of the NMR sample even though the protein does not contain any cysteines. When DTT was omitted, the protein was highly aggregated. However, in the presence of 10 mM DTT no signs of aggregation were observed.

NMR spectroscopy

All NMR spectra were recorded at 35 °C on a Bruker AMX600 spectrometer equipped with a triple-resonance gradient probe. The water suppression technique was either presaturation during the recycle delay or gradient water suppression via the WATERGATE sequence and homo-spoil pulses (Bax and Pochapsky, 1992; Sklenář et al., 1993). Quadrature detection in the indirectly detected dimensions was obtained in all cases using the TPPI-States method (Marion et al., 1989a).

Spectra were processed using the NMRPipe software package (Delaglio et al., 1995) and analyzed with PIPP (Garrett et al., 1991), NMRPipe and PEAK-SORT, an in-house software package. When appropriate, data processing included a solvent filter, zero-padding of the data to a power of 2, linear predicting back one data point of indirectly acquired data to obtain zero (zero and first order) phase corrections, and linear prediction of additional points for the indirectly acquired dimensions to increase resolution. Linear prediction by means of the mirror image technique was used only for constant-time experiments. In all cases, data were processed with a skewed sine-bell apodization function and one zero-filling was used in all dimensions.

Peak heights were automatically assigned for each residue in all 2D spectra after semiautomatically peak picking one 2D spectrum using NMRPipe. T_1 and T_2 values were determined by fitting the measured peak heights to the two-parameter profile $I(t) = I_0 \exp(-t/T_n)$. The Levenberg–Maquardt algorithm (Press et al., 1986) was used to determine the optimum values of T_n by minimizing the goodness of fit parameter, $\chi^2 = \Sigma(I_c(t) - I_e(t))^2/\sigma$, where $I_c(t)$ are the intensities calculated from the fitting parameters, $I_e(t)$ are the experimental intensities and σ is the standard deviation of the experimental intensities. The standard deviation was set to the root-mean-square base-

TABLE 1
ACQUISITION PARAMETERS FOR NMR EXPERIMENTS ON MMP-1

Experiment	Nucleus			No. of complex points			Spectral width (ppm)			Reference (ppm)		
	F1	F2	F3	F1	F2	F3	F1	F2	F3	F1	F2	F3
T_1, T_2, NOE HSQC	^{15}N	^{1}H		160	512		28.35	13.44		115.2	4.75	
CBCA(CO)NH	^{13}C	^{15}N	^{1}H	52	32	512	55.97	28.35	13.44	47.0	115.2	4.75
CBCANH	^{13}C	^{15}N	^{1}H	52	32	512	55.97	28.35	13.44	47.0	115.2	4.75
C(CO)NH	^{13}C	^{15}N	^{1}H	52	32	512	55.97	28.35	13.44	47.0	115.2	4.75
HBHA(CO)NH	^{1}H	^{15}N	^{1}H	52	32	512	6.67	28.35	13.44	4.75	115.2	4.75
HC(CO)NH	^{1}H	^{15}N	^{1}H	52	32	512	6.67	28.35	13.44	4.75	115.2	4.75
HNHA	^{1}H	^{15}N	^{1}H	48	21	512	9.50	27.59	13.44	4.75	115.2	4.75
HNCO	$^{13}C'$	^{15}N	^{1}H	64	32	512	12.00	21.92	13.44	177.0	115.2	4.75
HCACO	$^{13}C'$	^{13}C	^{1}H	64	15	512	12.00	15.06	8.42	177.0	56.0	4.75
HNCA	^{13}C	^{15}N	^{1}H	54	32	512	31.86	28.35	13.44	54.0	115.2	4.75
HCCH-COSY	^{1}H	^{13}C	^{1}H	128	22	256	8.42	20.71	8.42	2.6	43.0	2.6
HCCH-TOCSY	^{1}H	^{13}C	^{1}H	128	32	256	8.42	20.71	8.42	2.6	43.0	2.6
^{15}N-edited NOESY	^{1}H	^{15}N	^{1}H	128	32	512	13.44	28.35	13.44	4.75	115.2	4.75
^{13}C-edited NOESY	^{1}H	^{13}C	^{1}H	128	32	512	9.16	20.71	9.16	4.0	64.0	4.00

line noise in the spectra as determined from NMRDraw. Uncertainties in the T_1 and T_2 measurements were obtained from the covariance matrix generated in the Levenberg–Maquardt algorithm and were used in the Monte Carlo simulation for determining the standard deviations for fitting parameters (Kamath and Shriver, 1989; Palmer et al., 1991; Farrow et al., 1994).

The steady-state NOE values were determined from the ratios of the intensities of the peaks with and without proton saturation. The standard deviation of the NOE value was determined by the baseline noise (Farrow et al., 1994). The overall correlation time was determined by using residues that had ^{15}N T_1/T_2 ratios within one standard deviation and NOE values of greater than 0.6 (Kay et al., 1989; Clore et al., 1990a; Clubb et al., 1995). Three models of the spectral density functions were used to classify five classes of optimized parameters (Kay et al., 1989; Clore et al., 1990a,b; Farrow et al., 1994). Selection of the appropriate spectral density function was determined by initially fitting the data to the simplest spectral density function and only selecting a more complicated spectral density function as required to fit the data (Clore et al., 1990a; Powers et al., 1992a,b; Clubb et al., 1995).

The assignments of the ^1H, ^{15}N, ^{13}CO and ^{13}C resonances were based on the following experiments: CBCA-(CO)NH (Grzesiek and Bax, 1992a), CBCANH (Grzesiek and Bax, 1992b), C(CO)NH (Grzesiek et al., 1993), HC-(CO)NH (Grzesiek et al., 1993), HBHA(CO)NH (Grzesiek and Bax, 1993), HNCO (Grzesiek and Bax, 1992c), HCACO (Powers et al., 1991), HNHA (Vuister and Bax, 1993), HNCA (Kay et al., 1990), HCCH-COSY (Ikura et al., 1991) and HCCH-TOCSY (Bax et al., 1990). Table 1 summarizes the acquisition parameters for each of the experiments used in assigning the backbone and side-chain assignments for MMP-1 and for the secondary structure and dynamic analysis.

The secondary structure of MMP-1 is based on NOE data involving the NH, H^α and H^β protons from the ^{15}N- and ^{13}C-edited NOESY-HMQC experiments. The spectra were collected as described previously with 100 and 120 ms mixing times, respectively (Marion et al., 1989b,c). $^3J_{HN^\alpha}$ coupling constants were obtained from the relative intensity of H^α cross peaks to the NH diagonal in the HNHA experiment (Vuister and Bax, 1993). Coupling constants were measured with a scaling factor of 1.1 for relaxation. Slowly exchanging NH protons were identified by recording an HSQC spectrum 2 days after exchanging an MMP-1 sample from H_2O to D_2O.

The T_1 and T_2 data for MMP-1 were collected with 32 transients per increment. The T_1 inversion recovery times were 20, 60, 140, 240, 360, 520, 720 and 1200 ms and the T_2 Carr–Purcell–Meiboom–Gill (CPMG) (Meiboom and Gill, 1958) trains were 8, 24, 40, 56, 72, 104, 152 and 184 ms in duration (Markley et al., 1971; Kay et al., 1992). The recycle delays for the T_1 and T_2 experiments were 1.7 and 1.3 s, respectively. Since the NOE measurement requires an equilibrated ^{15}N magnetization for accurate analysis, the recycle time was extended to more than 6 s while collecting 48 transients per increment. In the NOE experiment with presaturation, the proton saturation period was 3 s. ^1H saturation was carried out with the use of 180° ^1H pulses applied every 5 ms.

Results and Discussion

Enzyme activity

Obtaining the NMR assignments, secondary structure and dynamic data for MMP-1 was dependent on optimizing the conditions of the NMR sample. The obvious difficulty in determining the NMR structure of inhibitor-free MMP-1 is the degradation of the NMR sample caused by self-cleavage of the enzyme. Since structural information is only relevant for an active enzyme, the NMR sample conditions must maintain enzyme activity while slowing down or possibly eliminating degradation of the enzyme.

The activity and structure of MMP-1 is dependent on the presence of both zinc and calcium with a stoichiometry of two zincs and one calcium (Lowry et al., 1992; Feng et al., 1995; Springman et al., 1995). Mass spectral analysis of matrilysin indicates that the metal association stoichiometry of the free enzyme is dependent on pH (Feng et al., 1995). At pH 7.0 matrilysin maintains both zinc metal ions and the enzyme is fully active, while at pH 6.0 the enzyme only contains one bound zinc suggesting a loss of the catalytic zinc and a diminished activity. This is also consistent with the observation that both collagenase and gelatinase exhibit bell-shaped dependencies on pH for V_{max} and V_{max}/K_m (Stack and Gray, 1990). A similar effect of pH on the activity of MMP-1 was seen in our laboratory. Reducing the pH of Bis-Tris buffer from 7.5 to 7.0 to 6.5 to 6.0 resulted in the specific activity of the enzyme (μmol/(min mg)) dropping from 24.2 to 22.4 to 21.6 to 19.2, respectively. The enzyme activity was 16% less at pH 7.5 in Tris-base versus Bis-Tris. Interestingly, the degree of inhibition by a small molecule inhibitor was not affected by either pH or type of buffer. However, the nature of the buffer had a significant effect on MMP-1's activity. The protein's V_{max} decreased significantly when a phosphate buffer was used. Apparently, the phosphate was chelating the active-site zinc and decreasing the enzyme's activity. In addition, the effect of DTT on MMP-1 activity was also analyzed. The specific activity of MMP-1 (28–81 nM) was determined over a range of DTT concentration (0–10 mM). At a 10:1 ratio of DTT to MMP-1, which is comparable to the NMR sample, the enzyme was completely active. Only at a very high DTT to MMP-1 ratio was an effect on MMP-1 activity observed. These results suggested that the use of deuterated Tris-base (which is readily available), 10

mM DTT and a pH of 6.5 for NMR studies would be reasonable compromises, resulting in a modest loss of enzyme activity and retention of the catalytic zinc.

Initial attempts to prepare an NMR sample that maintained the appropriate metal stoichiometry (1 mM MMP-1, 2 mM $ZnCl_2$ and 5 mM $CaCl_2$) resulted in precipitation of the protein with $ZnCl_2$ concentrations >0.1 mM. It is important to note that $ZnCl_2$ was not added to the enzyme activity measurements described above. Based on the observations of Gooley et al. (1993), zinc ligation of the histidine imidazole nitrogens is indicated by the presence of slowly exchanging imidazole NH protons where the imidazole nitrogen chemical shifts are in the range of 169–178 ppm. In the case of MMP-1, we observed four such histidine imidazole correlations in the HSQC spectra, where two correlations were approximately twice as intense as the remaining correlations, suggesting possible chemical shift degeneracy. This is consistent with the presence of two zinc atoms bound to MMP-1 where three histidine residues are ligated to each zinc atom. The presence of the catalytic zinc is also consistent with the observation that an autolysis product is observed over a period of 1–2 months by the appearance of new random-coil peaks in the ^{1}H-^{15}N HSQC spectra and that an inhibitor which binds to the catalytic zinc binds to MMP-1 under these NMR conditions.

An initial NMR spectrum of MMP-1 was extremely broadened, which is indicative of protein aggregation. Increasing the sample temperature or adjusting the $ZnCl_2$ concentration resulted in minimal improvement in the quality of the NMR spectra. Based on our previous success using DTT in improving the quality of the FGF-2 spectra (Moy et al., 1995), 10 mM DTT was added to the MMP-1 sample. This resulted in a dramatic improvement in the quality of the NMR spectra (Fig. 1). The mechanism of DTT in inhibiting MMP-1 aggregation is unknown, but may act similar to glycerol as a protein stabilizing agent by decreasing the water activity (Gekko and Timasheff, 1981a,b). The final NMR sample conditions of 10 mM Tris-base pH 6.5, 100 mM NaCl, 5 mM $CaCl_2$,

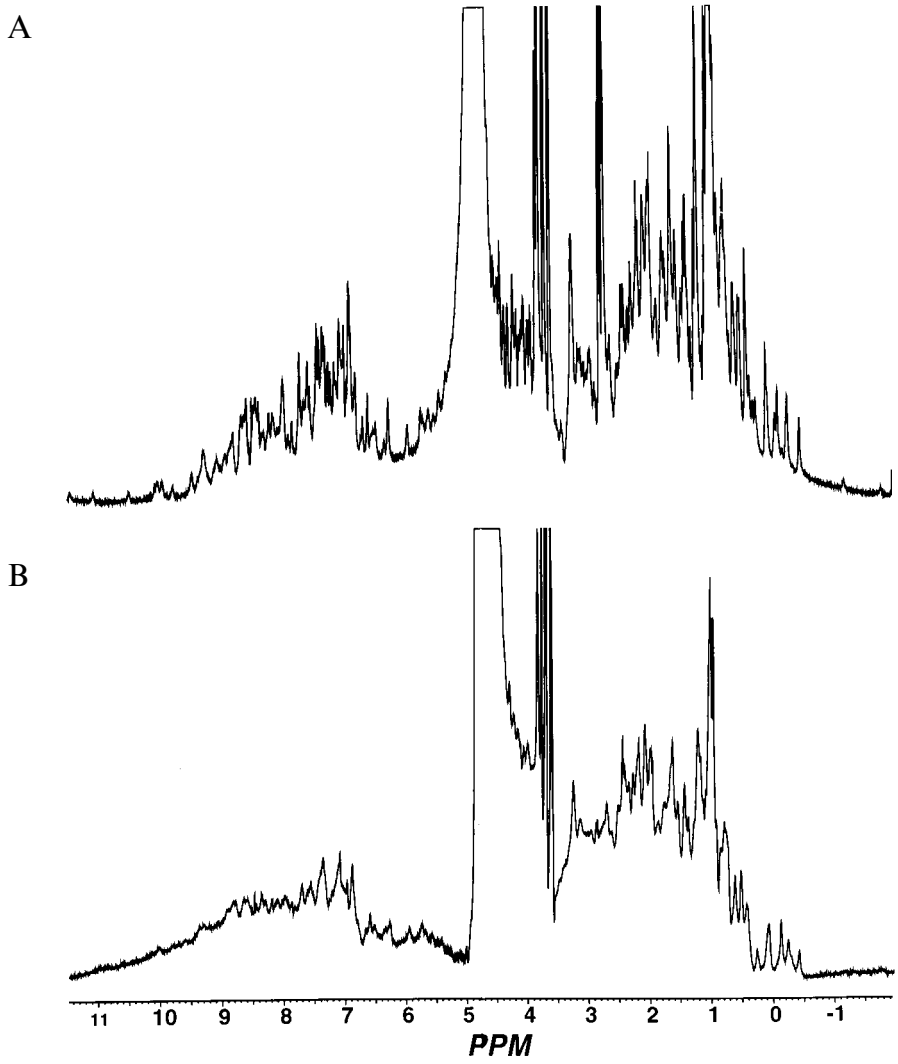

Fig. 1. 1D spectra of MMP-1 at 35 °C with DTT (A) and without DTT (B).

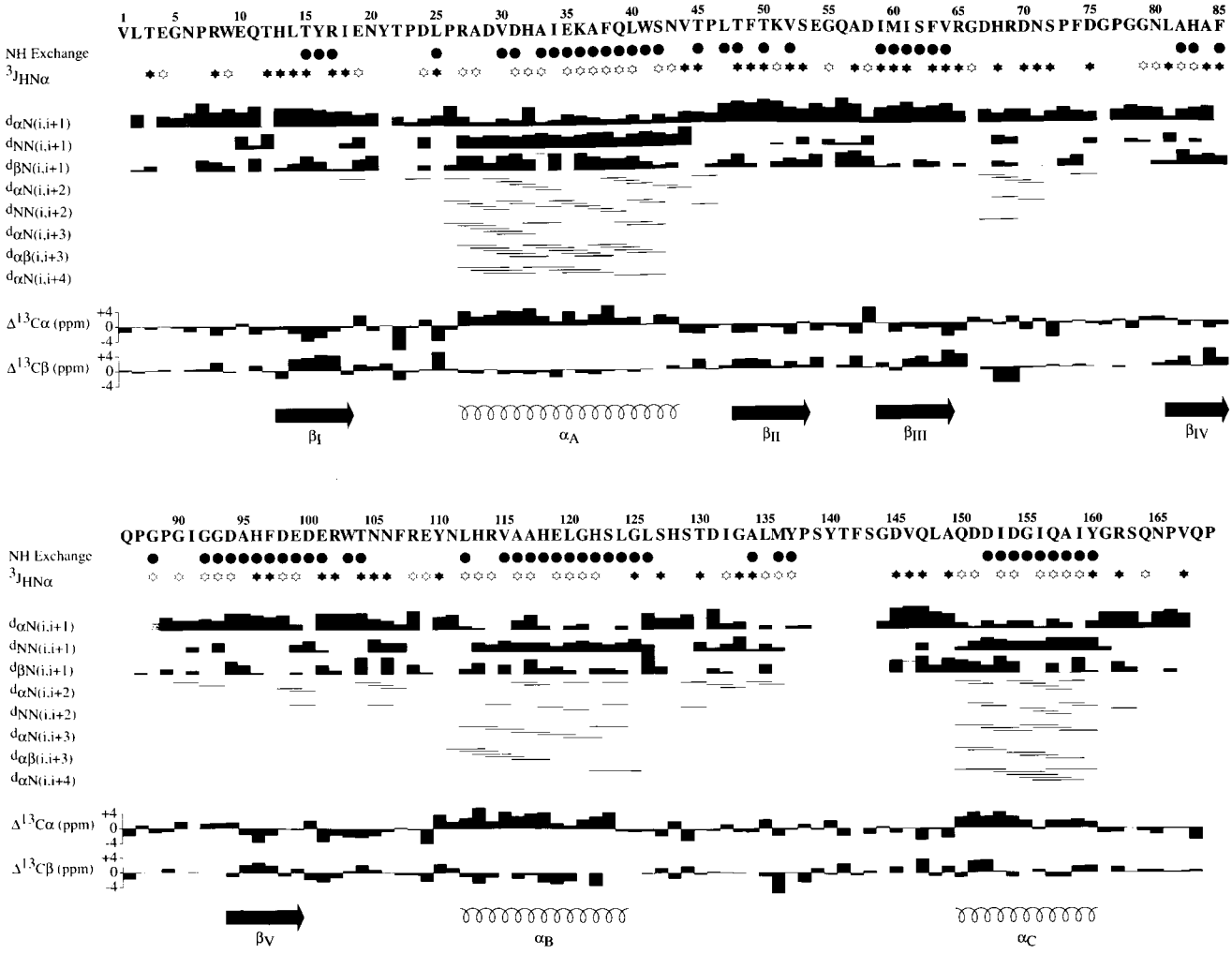

Fig. 2. Summary of the sequential and medium-range NOEs involving the NH, H^{α} and H^{β} protons, the amide exchange and $^3J_{HN^{\alpha}}$ coupling constant data, and the $^{13}C^{\alpha}$ and $^{13}C^{\beta}$ secondary chemical shifts observed for MMP-1 with the secondary structure deduced from these data. The thickness of the lines reflects the strength of the NOEs. Amide protons still present 24 h after exchange to D_2O are indicated by closed circles. The filled and open stars indicate $^3J_{HN^{\alpha}}$ values >8 Hz and <6 Hz, respectively. The open boxes represent potential sequential assignment NOEs that are obscured by resonance overlap and could therefore not be assigned unambiguously. The gray boxes on the same line as the H^{α}(i)-NH(i+1) NOEs represent the sequential NOE between the H^{α} proton of residue i and the $C^{\delta}H$ proton of the i+1 proline and are indicative of a *trans*-proline.

0.1 mM $ZnCl_2$, 2 mM NaN_3 and 10 mM DTT resulted in a properly folded and active protein sample which was stable for approximately 1–2 months at 35 °C.

Resonance assignments

The sequential assignments of MMP-1 essentially followed the semiautomated protocol described previously (Garrett et al., 1991; Powers et al., 1992a,b; Friedrichs et al., 1994). The assignments were based primarily on the correlations observed in four triple-resonance experiments (CBCA(CO)NH, CBCANH, HNHA and HBHA(CO)-NH) and by residue typing based on C^{α} and C^{β} chemical shifts (Grzesiek et al., 1993; Grzesiek and Bax, 1993) and verified by the correlations observed in the HCACO, HNCO and HNCA experiments and by the NOE patterns in the ^{15}N-edited NOESY spectra. The ^{13}C and ^1H side-chain assignments were based on a combination of correlations observed from the CBCA(CO)NH, HBHA-(CO)NH, C(CO)NH, HC(CO)NH and the HCCH-COSY experiments, where the aromatic side-chain assignments were obtained from the 3D ^{13}C-edited NOESY spectrum from intraresidue NOEs from the aromatic ring protons to the H^{α} and H^{β} protons and the amide side-chain assignments of asparagine and glutamine were obtained from the intraresidue NOEs from the NH_2 protons to the H^{β} and $C^{\gamma}H$ protons in the 3D ^{15}N-edited NOESY spectrum.

In general, the sequential assignments for MMP-1 were relatively straightforward because of the high quality of the NMR spectra. There were two minor obstacles to overcome in order to complete the MMP-1 assignments: (i) there were a total of 11 prolines in the sequence which were closely clustered, resulting in short (1–3) intervening sequences; and (ii) a lack of data for residues Phe[142]–

Gly[144] made the assignments in this region problematic. Particularly, no cross peaks were observed in the 2D ^{1}H-^{15}N HSQC spectra or in any 3D NMR spectra based on NH correlations, but spin systems were observed in the HCCH-COSY and ^{13}C-edited NOESY spectra. Therefore, the assignments in these regions were completed by elimination, i.e. Phe[142] and Ser[143] were assigned from the remaining phenylalanine and serine spin systems in the HCCH-COSY spectra. The accuracies of these assignments were verified by consistency with the structure refinement of MMP-1 using the ^{15}N- and ^{13}C-edited NOESY spectra. The ^{1}H, ^{15}N, ^{13}C and ^{13}CO sequential resonance assignments are provided in Table S1 (supplementary material) and are deposited in the BioMagRes Databank (Seavey et al., 1991).

Secondary structure

The regular secondary structure elements of MMP-1 were identified from a qualitative analysis of sequential and interstrand NOEs, NH exchange rates, $^{3}J_{HN\alpha}$ coupling constants (Clore and Gronenborn, 1989) and the $^{13}C^{\alpha}$ and $^{13}C^{\beta}$ secondary chemical shifts (Spera and Bax, 1991). These data, together with the deduced secondary structure elements, are summarized in Fig. 2. The sequential and medium-range NOEs were obtained from a qualitative analysis of the ^{15}N- and ^{13}C-edited NOESY spectra, where box heights are related to peak intensity. $^{3}J_{HN\alpha}$ coupling constants were measured for 143 of the 152 assigned non-proline residues, and 68 of the 152 assigned non-proline amide protons were identified as very slow exchanging amide protons.

It is apparent from the data in Figs. 2 and 3 that the MMP-1 structure is composed of a five-stranded mixed parallel and antiparallel β-sheet (where strand I extends from residues 13 to 19, strand II from 48 to 52, strand III from 59 to 65, strand IV from 82 to 85 and strand V from 94 to 99) and three α-helices (where helix A corresponds to residues 27–43, helix B corresponds to residues 112–123 and helix C corresponds to residues 150–160).

Comparison of the NMR and X-ray structure

Comparison of the solution NMR secondary structure of inhibitor-free MMP-1 with the X-ray crystal structures of MMP-1 complexed with inhibitors indicates essentially the same secondary structure (Borkakoti et al., 1994; Lovejoy et al., 1994a; Spurlino et al., 1994). Helix A and

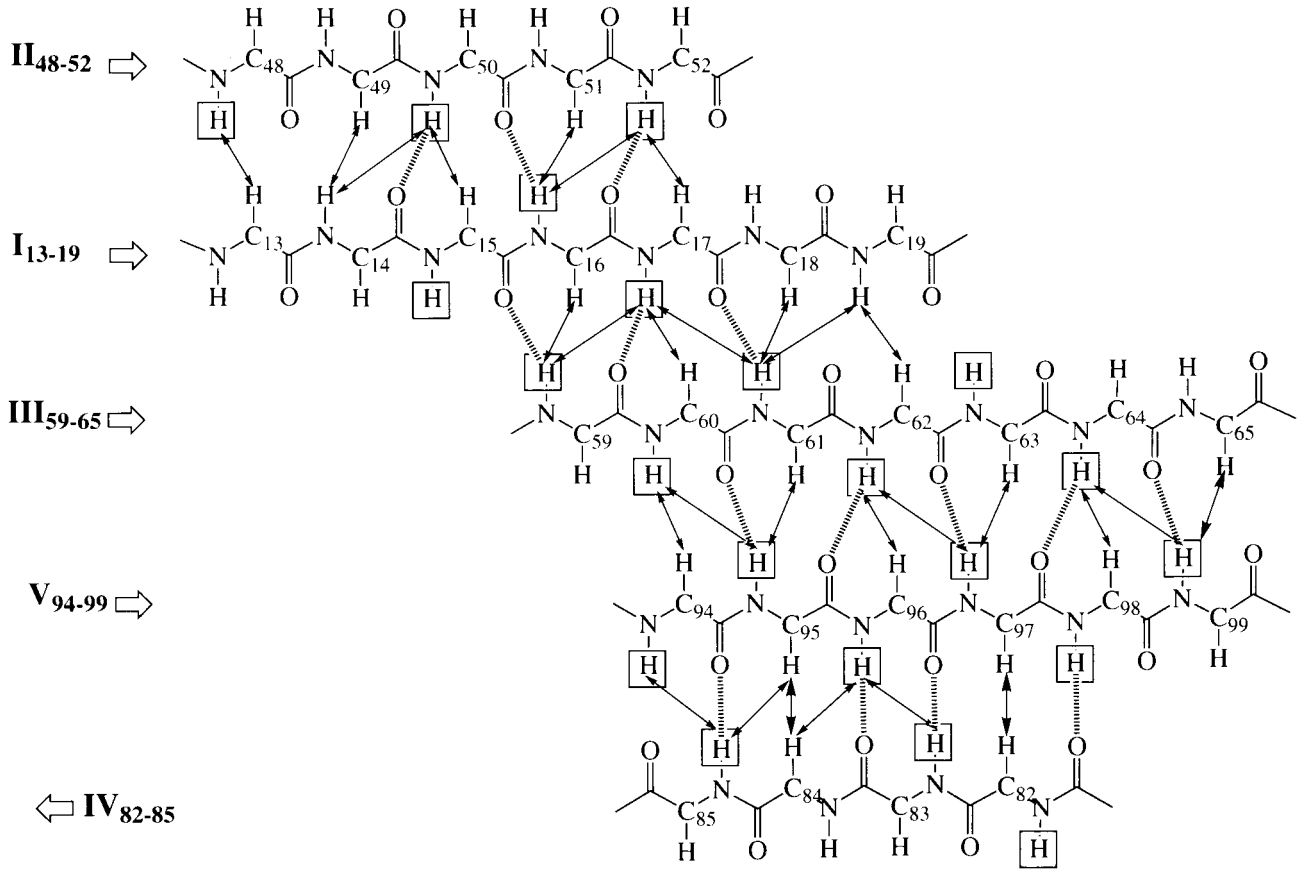

Fig. 3. Secondary structure elements of MMP-1 as determined from qualitative analysis of the NOE and amide exchange data. The β-strands are indicated on the left by Roman numerals and the residue number range. Interstrand NOEs derived from the 3D ^{15}N- and ^{13}C-edited NOESY spectra are indicated by arrows, and slowly exchanging amide protons are boxed. The hydrogen bonds deduced from these data are shown as broken lines.

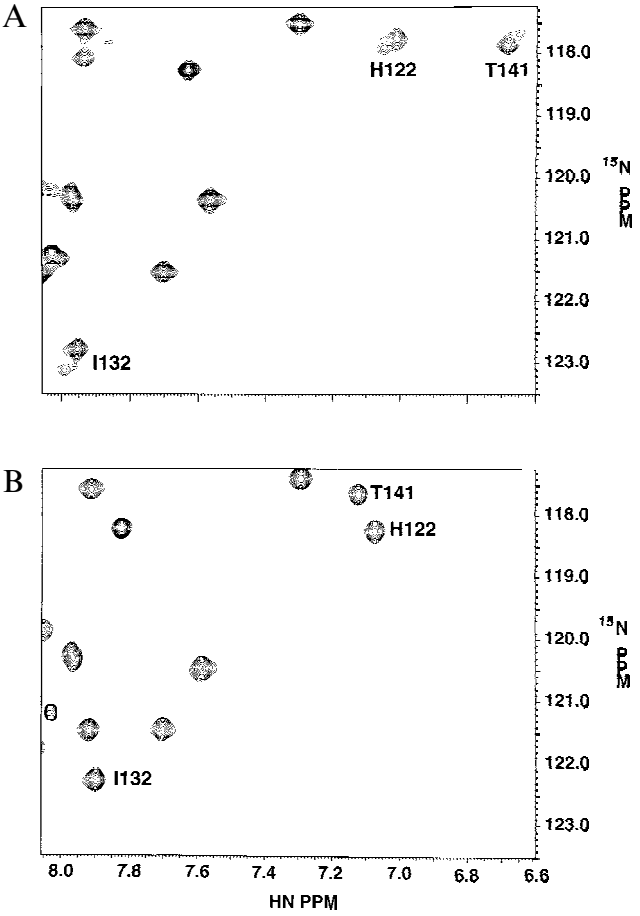

Fig. 4. Expanded region of the ^{1}H-^{15}N HSQC spectra of (A) free MMP-1 and (B) inhibited MMP-1. Residues with double peaks in the free spectra are labeled.

β-strand I are one residue longer in the NMR structure and β-strand V starts at residue 95 and ends at residue 98 in the X-ray structure compared to residues 94 and 99 in the NMR structure.

An X-ray structure of MMP-1 in the absence of an inhibitor has also been reported (Lovejoy et al., 1994b). This structure is unique because MMP-1 forms a dimer where the active site is occupied with the N-terminus of its neighbor such that L2 ligates the catalytic zinc, T3 is buried in the hydrophobic P1' pocket and E4 and G5 are in an extended conformation filling the remainder of the active site. Apart from the N-terminus, the rms deviation between MMP-1 in the dimer form and other inhibited MMP-1 X-ray structures is very low. It is quite clear that the X-ray structure of the MMP-1 dimer complex should be treated as a unique inhibited complex and not as a structure of inhibitor-free MMP-1. Also, the MMP-1 dimer structure does not suggest that the active form of MMP-1 is a dimer; in fact, it might suggest that MMP-1 dimer formation may inhibit MMP-1 activity. Since the evidence indicates that DTT does not affect MMP-1 activity, the current study represents unique information on the structure of inhibitor-free MMP-1 where the use of DTT to prevent MMP-1 dimerization or aggregation is not forcing the protein into an unnatural and irrelevant state as evident by the activity of the protein.

From the X-ray structures of MMP-1, the active site is formed by β-strand IV, helix B and a random-coil region to the C-terminus of helix B where the catalytic zinc is ligated by His^{118}, His^{122} and His^{128} (Borkakoti et al., 1994; Lovejoy et al., 1994a,b; Spurlino et al., 1994). From an analysis of the NMR data for ligand free MMP-1, it appears that a major effect an inhibitor may have on the MMP-1 structure is a modification of the local mobility. This is apparent from the observation that a number of residues which comprise the MMP-1 active site appear as doublets in the ^{1}H-^{15}N HSQC spectra and this doublet characteristic disappears in the presence of an inhibitor (Figs. 4 and 5). These residues correspond to His^{96}, Trp^{103}, Leu^{112}, Val^{115}, Ala^{116}, His^{118}, Glu^{119}, Gly^{121}, His^{122}, Leu^{124}, Gly^{125}, His^{128}, Thr^{130}, Asp^{131}, Ile^{132}, Leu^{135} and Thr^{141}. The observed doublets in the ^{1}H-^{15}N HSQC spectra might be the result of a slow conformational change in the active site that results in a concerted motion of helix B (112–123), the zinc ligated histidines (118,122,128) and the nearby loop region. This may explain why Trp^{103} and His^{96} are affected since the side chain of Trp^{103} and the backbone of His^{96} are in close proximity to helix B in the X-ray structure and would follow the motion of helix B. If the hinge point of this motion is the zinc ligated histidines, when an inhibitor binds by chelating the zinc it may effectively remove this motion while maximizing the inhibitor's interaction with β-strand IV. It is also plausible that the observed HSQC doublets are a result of DTT. DTT might form a shell in the active site which slowly exchanges with water, so the HSQC doublet would result from an NH being in the vicinity of either water or DTT. This seems unlikely since *all* the HSQC doublets disappear in the presence of the inhibitor, which is not large enough to directly interact or displace the DTT from all the residues exhibiting an HSQC doublet in inhibitor-free MMP-1.

In addition, residues Pro^{138}–Gly^{144} are poorly defined based on the ^{15}N-edited NOESY spectra and residues Phe^{142}–Gly^{144} did not exhibit a cross peak in the ^{1}H-^{15}N HSQC spectra. In the presence of an inhibitor, this region is still poorly defined and the only new cross peak observed in the ^{1}H-^{15}N HSQC spectra of the complex is for Gly^{144}. It is important to point out that the B-factor for these residues in the X-ray structure of inhibited MMP-1 is relatively small and consistent with the remainder of the protein (Borkakoti et al., 1994; Lovejoy et al., 1994a,b; Spurlino et al., 1994). This indicates that the X-ray structures of inhibited MMP-1 might be misleading, and the defined structure for residues Pro^{138}–Gly^{144} and the corresponding interaction with the inhibitor may only be a result of crystallization and inconsequential for inhibitor binding. Of course, the interaction to residues

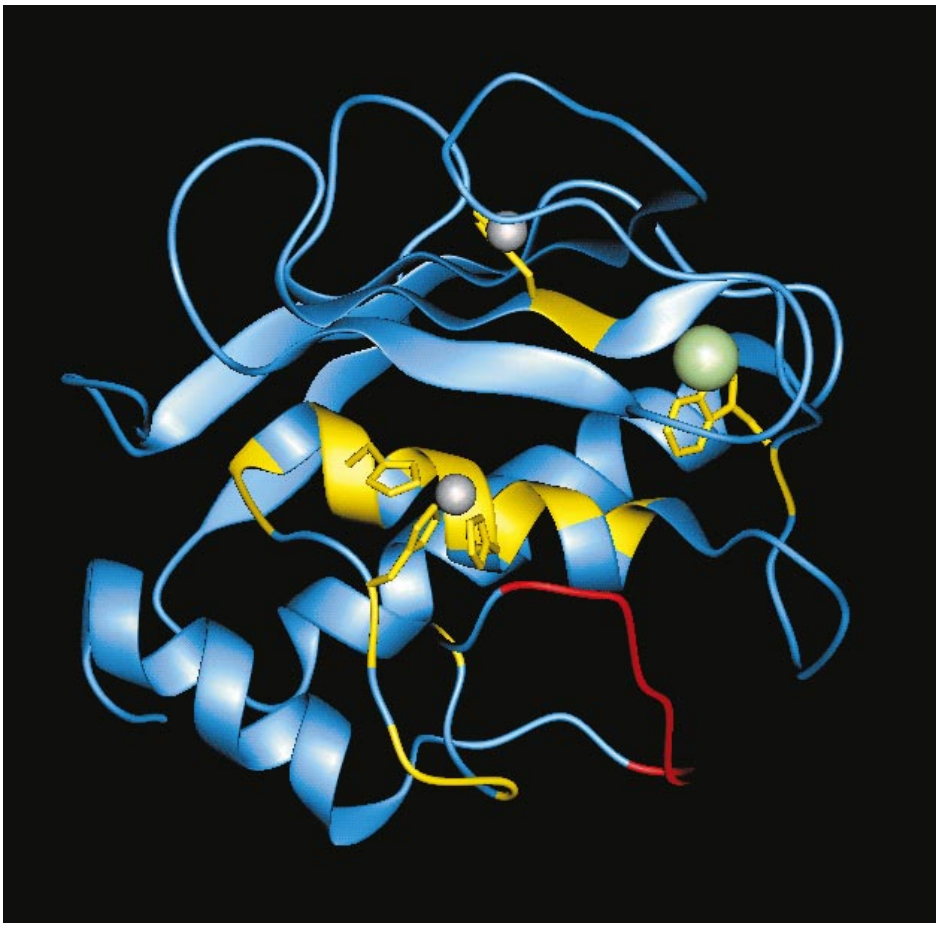

Fig. 5. Ribbon diagram of the X-ray structure of MMP-1, with residues exhibiting a doubling of peaks in the ^{1}H-^{15}N HSQC colored yellow and disordered residues Pro^{138}–Gly^{144} colored red. Side chains for His^{96}, His^{118}, His^{122}, His^{128} and Trp^{103} are shown. The zinc and calcium ions are shown as van der Waals spheres.

Pro^{138}–Gly^{144} may very well be inhibitor dependent. The inhibitor used in this NMR study of collagenase is a sulfonamide derivative of a hydroxamic acid compound. This inhibitor binds similar to other compounds in this series where the hydroxamic acid chelates the catalytic zinc and the remainder of the compound is located in both the S1' and S2' binding pockets; binding in the S2' pocket is not very deep. The right-handed orientation of the inhibitor is based on strong chemical shift perturbations and preliminary NOEs to residues in this region of the protein. In particular, large chemical shift perturbations in the ^{1}H-^{15}N HSQC spectra were observed for residues Asn^{80}–Ala^{84}, Val^{115} and His^{118}, and NOEs from both a 3D ^{15}N-edited NOESY and a 2D $^{15}N/^{13}C$-filtered NOESY were observed between the inhibitor and Leu^{81}, Ala^{82} and Val^{115}. No interactions were observed between the inhibitor and residues Pro^{138}–Gly^{144}, but a ^{1}H-^{15}N HSQC cross peak for Gly^{144} is only present in the complex.

These results suggest that the active site for inhibitor-free MMP-1 is significantly more mobile than implied by the X-ray structures of MMP-1 in the presence of an inhibitor. In particular, it suggests that helix B and the ligated zinc may be in a slow conformational exchange and that the random-coil region in the vicinity of the active site has a high order of mobility to the extent that the NH protons for Phe^{142}–Gly^{144} are broadened beyond detection. These results may also suggest that a significant factor in the ability of a ligand to inhibit MMP-1 activity may be its capacity to stabilize the mobile active site.

Dynamics of free and inhibited MMP-1

To further substantiate the observed mobility of the active site of inhibitor-free MMP-1, ^{15}N T_1, T_2 and NOE data were collected for free and inhibited MMP-1 (data not shown). The overall correlation times for both free and inhibited MMP-1 were essentially identical, 9.7 ± 0.3 and 9.6 ± 0.3 ns, respectively. The generalized order parameter (S^2) is plotted as a function of residue number for both free and inhibited MMP-1 in Fig. 6. It is readily apparent from Fig. 6 that the calculated order parameters are nearly identical for both free and inhibited MMP-1. The average values of the order parameter S^2 (excluding

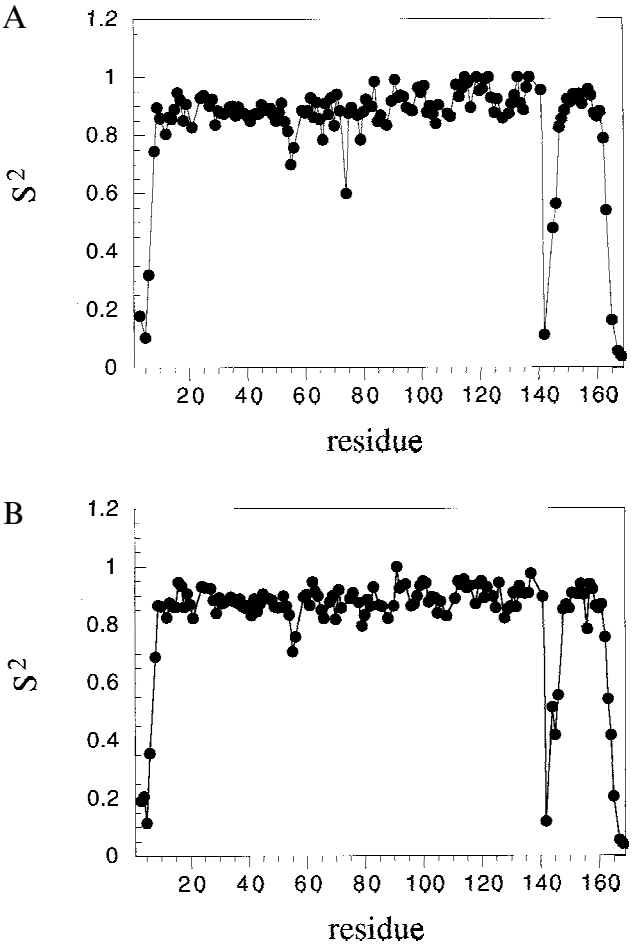

Fig. 6. Plots of S^2 on a per residue basis for (A) free MMP-1 and (B) inhibited MMP-1.

residues 1–7, 138–144 and 163–169) for free MMP-1 and inhibited MMP-1 are 0.89 ± 0.06 and 0.88 ± 0.05, respectively, indicating a limited conformational flexibility for most of the protein. These results also indicate that residues Pro^{138}–Gly^{144}, in addition to the residues at the N- and C-terminus, are highly mobile in both the free and inhibited MMP-1 samples with $S^2 \leq 0.6$. This is consistent with the previous observation that these residues are inherently mobile and that no significant interaction with the inhibitor occurs.

As previously reported in the inhibited MMP-1 X-ray structure (Spurlino et al., 1994), an inhibitor may extend the formation of a β-sheet between β-strand IV and the disordered residues corresponding to Pro^{138}–Gly^{144}. This is consistent with the NMR structure of stromelysin complexed with an *N*-carboxyl alkyl inhibitor (Gooley et al., 1994) where the corresponding loop region in stromelysin is well defined and strong NOEs are observed between the inhibitor and residues 139–140. This differs significantly from the results reported here. The loop region corresponding to residues Pro^{138}–Gly^{144} is highly disordered, with no observable contact between collagenase and the inhibitor in this region. This suggests that the interaction to the Pro^{138}–Gly^{144} loop region is either inhibitor dependent, an artifact of crystallization or, in the case of the NMR structures, subtle differences between the active sites of collagenase and stromelysin in addition to inhibitor differences. In either case, it demonstrates that the Pro^{138}–Gly^{144} loop region is highly mobile and that the interaction of an inhibitor with this loop region, while beneficial, is not crucial for binding to the protein.

For residues which exhibited a doubling of ^1H-^{15}N HSQC peaks in free MMP-1, little effect on the generalized order parameters ($S^2 \geq 0.8$) was observed for the complex compared to the major peaks in free MMP-1. All these residues were fitted to the simplified spectral density function where $\tau_e \leq 20$ ps. This suggests that the predominate motion observed for these residues in free MMP-1 is the slow exchange between two distinct conformations, resulting in the peak doubling observed in the HSQC spectra, while the presence of the inhibitor results in a single preferred conformation. This conformational exchange, in addition to the high mobility for residues Pro^{138}–Gly^{144}, indicates an inherent flexibility in the protein and suggests that the motion in this region may be crucial for proper inhibitor binding.

Conclusions

Nearly complete ^1H, ^{15}N, ^{13}C and ^{13}CO resonance assignments for the inhibitor-free catalytic fragment of human MMP-1 have been determined by 3D triple-resonance heteronuclear NMR experiments. The secondary structure elements present in MMP-1 have been identified based on a qualitative analysis of sequential and interstrand NOEs, NH exchange rates, $^3J_{HN^\alpha}$ coupling constants and the $^{13}C^\alpha$ and $^{13}C^\beta$ secondary chemical shifts. In general, the NMR structure agrees with the X-ray structures of inhibited MMP-1, where the protein is composed of a mixed parallel and antiparallel five-stranded β-sheet and three α-helices. The major distinction between the NMR structure of inhibitor-free MMP-1 and the X-ray structures of inhibited MMP-1 is the observation that the residues which comprise the active site appear to be more mobile in the free MMP-1 NMR structure as evident by a doubling of peaks in the ^1H-^{15}N HSQC spectra, the lack of information in the ^{15}N-edited NOESY spectra and the observed order parameters (S^2). The inherent mobility of the MMP-1 active site has significant implication in drug design.

Acknowledgements

We would like to thank Dr. Dan Garrett and Frank Delaglio for the use of their programs for NMR data analysis and processing, and Dr. Neil Farrow for the use of his programs for the analysis of ^{15}N relaxation data.

References

Bax, A., Clore, G.M. and Gronenborn, A.M. (1990) *J. Magn. Reson.*, **88**, 425–431.

Bax, A. and Pochapsky, S.S. (1992) *J. Magn. Reson.*, **99**, 638–643.

Becker, J.W., Marcy, A.I. and Rokosz, L.L. (1995) *Protein Sci.*, **4**, 1966–1976.

Bode, W., Reinemer, P., Huber, R., Kleine, T., Schnierer, S. and Tschesche, H. (1994) *EMBO J.*, **13**, 1263–1269.

Borkakoti, N., Winkler, F.K., Williams, D.H., D'Arcy, A., Broadhurst, M.J., Brown, P.A., Johnson, W.H. and Murray, E.J. (1994) *Nat. Struct. Biol.*, **1**, 106–110.

Botos, I., Scapozza, L., Zhang, D., Liotta, L.A. and Meyer, E.F. (1996) *Proc. Natl. Acad. Sci. USA*, **93**, 2749–2754.

Broutin, I., Arnoux, B., Riche, C., Lecroisey, A., Keil, B., Pascard, C. and Ducruix, A. (1996) *Acta Crystallogr.*, **D52**, 380–392.

Clore, G.M. and Gronenborn, A.M. (1989) *Crit. Rev. Biochem. Mol. Biol.*, **24**, 479–564.

Clore, G.M., Driscoll, P.C., Wingfield, P.T. and Gronenborn, A.M. (1990a) *Biochemistry*, **29**, 7387–7401.

Clore, G.M., Szabo, A., Bax, A., Kay, L.E., Driscoll, P.C. and Gronenborn, A.M. (1990b) *J. Am. Chem. Soc.*, **112**, 4989–4991.

Clubb, R.T., Omichinski, J.G., Sakaguchi, K., Appella, E., Gronenborn, A.M. and Clore, G.M. (1995) *Protein Sci.*, **4**, 855.

Delaglio, F., Grzesiek, S., Vuister, G.W., Zhu, G., Pfeifer, J. and Bax, A. (1995) *J. Biomol. NMR*, **6**, 277–293.

Farrow, N.A., Muhandiram, R., Singer, A.U., Pascal, S.M., Kay, C.M., Gish, G., Shoelson, S.E., Pawson, T., Forman-Kay, J.D. and Kay, L.E. (1994) *Biochemistry*, **33**, 5984–6003.

Feng, R., Castelhano, A.L., Billedeau, R. and Yuan, Z. (1995) *J. Am. Soc. Mass Spectrom.*, **6**, 1105–1111.

Friedrichs, M.S., Mueller, L. and Wittekind, M. (1994) *J. Biomol. NMR*, **4**, 703–726.

Garrett, D.S., Powers, R., Gronenborn, A.M. and Clore, G.M. (1991) *J. Magn. Reson.*, **95**, 214–220.

Gekko, K. and Timasheff, S.N. (1981a) *Biochemistry*, **20**, 4667–4676.

Gekko, K. and Timasheff, S.N. (1981b) *Biochemistry*, **20**, 4677–4686.

Goldberg, G.I., Wilhelm, S.M., Kronberger, A., Bauer, E.A., Grant, G.A. and Eisen, A.Z. (1986) *J. Biol. Chem.*, **261**, 6600–6605.

Gooley, P.R., Johnson, B.A., Marcy, A.I. and Cuca, G.C. (1993) *Biochemistry*, **32**, 13098–13108.

Gooley, P.R., O'Connell, J.F. and Marcy, A.I. (1994) *Nat. Struct. Biol.*, **1**, 111–118.

Gooley, P.R., O'Connell, J.F., Marcy, A.I., Cuca, G.C., Axel, M.G., Caldwell, C.G., Hagmann, W.K. and Becker, J.W. (1996) *J. Biomol. NMR*, **7**, 8–28.

Grymes, R.A., Kronberger, A. and Bauer, E.A. (1993) *Clin. Dermatol.*, **9**, 69–85.

Grzesiek, S. and Bax, A. (1992a) *J. Am. Chem. Soc.*, **114**, 6291–6293.

Grzesiek, S. and Bax, A. (1992b) *J. Magn. Reson.*, **99**, 201–207.

Grzesiek, S. and Bax, A. (1992c) *J. Magn. Reson.*, **96**, 432–440.

Grzesiek, S., Anglister, J. and Bax, A. (1993) *J. Magn. Reson.*, **B101**, 114–119.

Grzesiek, S. and Bax, A. (1993) *J. Biomol. NMR*, **3**, 185–204.

Ikura, M., Kay, L.E. and Bax, A. (1991) *J. Biomol. NMR*, **1**, 299–304.

Kamath, U. and Shriver, J.W. (1989) *J. Biol. Chem.*, **264**, 5586.

Kay, L.E., Torchia, D.A. and Bax, A. (1989) *Biochemistry*, **28**, 8972–8979.

Kay, L.E., Ikura, M., Tschudin, R. and Bax, A. (1990) *J. Magn. Reson.*, **89**, 496–514.

Kay, L.E., Nicholson, L.K., Delaglio, F., Bax, A. and Torchia, D.A. (1992) *J. Magn. Reson.*, **97**, 359–375.

Lovejoy, B., Cleasby, A., Hassell, A.M., Longley, K., Luther, M.A., Weigl, D., McGeehan, G., McElroy, A.B., Drewry, D., Lambert, M.H. and Jordan, S.R. (1994a) *Science*, **263**, 375–377.

Lovejoy, B., Hassell, A.M. and Luther, M.A. (1994b) *Biochemistry*, **33**, 8207–8217.

Lowry, C.L., McGeehan, G. and LeVine, H.I. (1992) *Proteins Struct. Funct. Genet.*, **12**, 42–48.

Marion, D., Driscoll, P.C., Kay, L.E., Wingfield, P.T., Bax, A., Gronenborn, A.M. and Clore, G.M. (1989a) *Biochemistry*, **28**, 6150–6156.

Marion, D., Ikura, M., Tschudin, R. and Bax, A. (1989b) *J. Magn. Reson.*, **85**, 393–399.

Marion, D., Kay, L.E., Sparks, S.W., Torchia, D.A. and Bax, A. (1989c) *J. Am. Chem. Soc.*, **111**, 1515–1517.

Markley, J.L., Horsley, W.J. and Klein, M.P. (1971) *J. Chem. Phys.*, **55**, 3604.

Meiboom, S. and Gill, D. (1958) *Rev. Sci. Instrum.*, **29**, 688.

Morphy, J.R., Millican, T.A. and Porter, J.R. (1995) *Curr. Med. Chem.*, **2**, 743–762.

Moy, F.J., Seddon, A.P., Campbell, E.B., Boehlen, P. and Powers, R. (1995) *J. Biomol. NMR*, **6**, 245–254.

Muller, D., Quantin, B., Gesnel, M.-C., Millon-Collard, R., Abecassis, J. and Breathnach, R. (1988) *Biochem. J.*, **253**, 187–192.

Palmer, A.G.I., Rance, M. and Wright, P.E. (1991) *J. Am. Chem. Soc.*, **113**, 4371.

Powers, R., Gronenborn, A.M., Clore, G.M. and Bax, A. (1991) *J. Magn. Reson.*, **94**, 209–213.

Powers, R., Clore, G.M., Stahl, S.J., Wingfield, P.T. and Gronenborn, A. (1992a) *Biochemistry*, **31**, 9150–9157.

Powers, R., Garrett, D.S., March, C.J., Frieden, E.A., Gronenborn, A.M. and Clore, G.M. (1992b) *Biochemistry*, **31**, 4334–4346.

Press, W.M., Flannery, B.P., Teukolsky, S.A. and Vetterling, W.T. (1986) *Numerical Recipes*, Cambridge University Press, Cambridge.

Ries, C. and Petrides, E. (1995) *Biol. Chem. Hoppe-Seyler*, **376**, 345–355.

Sambrook, S., Fritsch, E.F. and Maniatis, T. (1989) *Molecular Cloning: A Laboratory Manual*, Cold Spring Harbour Laboratory Press, New York, NY, U.S.A.

Seavey, B.R., Farr, E.A., Westler, W.M. and Markley, J.L. (1991) *J. Biomol. NMR*, **1**, 217–230.

Sklenář, V., Piotto, M., Leppik, R. and Saudek, V. (1993) *J. Magn. Reson.*, **A102**, 241–245.

Spera, S. and Bax, A. (1991) *J. Am. Chem. Soc.*, **113**, 5490–5492.

Springman, E.B., Nagase, H., Birkedal-Hansen, H. and Van Wart, H.E. (1995) *Biochemistry*, **34**, 15713–15720.

Spurlino, J.C., Smallwood, A.M., Carlton, D.D., Banks, T.M., Vavra, K.J., Johnson, J.S., Cook, E.R., Falvo, J., Wahl, R.C., Pulvino, T.A., Wendoloski, J.J. and Smith, D.L. (1994) *Proteins Struct. Funct. Genet.*, **19**, 98–109.

Stack, M.S. and Gray, R.D. (1990) *Arch. Biochem. Biophys.*, **281**, 257–263.

Stams, T., Spurlino, J.C., Smith, D.L., Wahl, R.C., Ho, T.F., Qoronfleh, M.W., Banks, T.M. and Rubin, B. (1994) *Nat. Struct. Biol.*, **1**, 119–123.

Van Doren, S.R., Kurochkin, A.V. and Ye, Q. (1993) *Biochemistry*, **32**, 13109–13122.

Van Doren, S.R., Kurochkin, A.V., Hu, W., Ye, Q.-Z., Johnson, L.L., Hupe, D.J. and Zuiderweg, E.R.P. (1995) *Protein Sci.*, **4**, 2487–2498.

Vuister, G.W. and Bax, A. (1993) *J. Am. Chem. Soc.*, **115**, 7772–7777.

Weingarten, H. and Feder, J. (1985) *Anal. Biochem.*, **147**, 437–440.

Woessner Jr., J.F. (1991) *FASEB J.*, **5**, 2145–2154.